AIP | Journal of Applied Physics

Thermal conductivity modeling of compacted type nanocomposites

Tse-Yang Hsieh, Jaw-Yen Yang, and Zuu-Chang Hong

Articles you may be interested in

Thermal transport in crystalline Si/Ge nano-composites: Atomistic simulations and microscopic models
Appl. Phys. Lett. **100**, 091903 (2012); 10.1063/1.3688943

Thermal conductivity modeling of circular-wire nanocomposites
J. Appl. Phys. **108**, 044306 (2010); 10.1063/1.3457230

Strain effect analysis on phonon thermal conductivity of two-dimensional nanocomposites
J. Appl. Phys. **106**, 114302 (2009); 10.1063/1.3259383

Thermal conductivity modeling of compacted nanowire composites
J. Appl. Phys. **101**, 054320 (2007); 10.1063/1.2653777

Thermal conductivity of tubular and core/shell nanowires
Appl. Phys. Lett. **89**, 063121 (2006); 10.1063/1.2336720

2014 Special Topics

PEROVSKITES
2D MATERIALS
MESOPOROUS MATERIALS
BIOMATERIALS/ BIOELECTRONICS
METAL-ORGANIC FRAMEWORK MATERIALS

AIP | APL Materials

Submit Today!

Thermal conductivity modeling of compacted type nanocomposites

Tse-Yang Hsieh,[1] Jaw-Yen Yang,[2,a)] and Zuu-Chang Hong[1]

[1]*Department of Mechanical and Electro-Mechanical Engineering, Tamkang University, Tamsui 25137, Taiwan*

[2]*Center for Quantum Science and Engineering, National Taiwan University, Taipei 10764, Taiwan*

Due to different interface densities and arrangements, the compacted type nanocomposites may yield even lower thermal conductivity than embedded type nanocomposites. In this paper, the phonon transport and thermal conductivity in compacted type nanocomposites (nanowires and nanoparticles) are investigated using a deterministic phonon Boltzmann transport equation solver. The effects of interface density and characteristic size on the phonon energy transport in nanocomposites are studied. It is found that the silicon-germanium compacted nanoparticle composites can have lower value of thermal conductivity than that of compacted nanowire composites under the same characteristic size (21.6% lower when the characteristic size is 3 nm). © 2009 American Institute of Physics. [DOI: 10.1063/1.3182803]

I. INTRODUCTION

Recent advances in synthesis, assembly, etching, processing, and microanalysis are enabling the routine production of well characterized materials with structure of nanometer-length scale. The feature size of electronic devices in current integrated circuits has become comparable to or even smaller than the mean free path (MFP) of the energy carrier and is projected to be much smaller in the near future. Examples are semiconductor quantum dots and superlattices, nanocomposites, multilayer coatings, and microelectronic and optoelectronic devices. Nanoscale structures attracted significant attention in recent years due to their importance in a variety of applications.[1–4]

Heat transport in semiconductors and insulators is mainly by lattice vibration. These vibrations travel within the medium as waves and can be regarded as pseudoparticles. This heat carrier is called phonon.[5] In many systems of current interest, the characteristic length scale of the microstructure is the same as the MFP of phonon and sometimes comparable to the phonon wavelength. This clearly necessitates an understanding of the nanoscale heat transport beyond that available at the continuum level, i.e., the Fourier conduction law.[6]

The efficiency of thermoelectric devices can be characterized by the nondimensional thermoelectric figure of merit $ZT = S^2 \sigma T / k$, where S is the Seebeck coefficient, σ is the electrical conductivity, k is the thermal conductivity, and T is the absolute temperature. Recent developments in highly efficient thermoelectric devices applied nanostructure-based materials such as Bi_2Te_3/Sb_2Te_3 superlattices[7] and PbTe/PbSeTe quantum dot superlattices,[8] and the marked increases in ZT values are mainly contributed by the reduction in phonon thermal conductivity. Thermal conductivity reduction is the major mechanism behind the enhanced figure of merit[9] and past studies on nanocomposites show that further reduction in thermal conductivity may be achieved due to higher interface density. Thus, nanocomposites can provide a pathway to scale up the interface effect that can greatly enhance the efficiency of thermoelectric devices.

Phonon energy transport in nanocomposite has recently been studied by several researchers.[10–16] Most of these efforts in simulating phonon heat transport are on composites with nanowires or nanoparticles embedded in a host matrix material. The host material forms a continuous phase in which nanowires or nanoparticles are dispersed. A deterministic phonon Boltzmann transport equation (BTE) solver was employed to study the phonon heat transfer and thermal conductivity of embedded nanowire composites[10,11] and embedded nanoparticle composites.[15] The Monte Carlo (MC) method was also employed to solve for compacted random nanowire composites[14] and embedded nanoparticle composites.[16] Cylindrical nanopore composites are studied based on analytic solutions of phonon BTE.[12,13]

Another possible interface arrangement of the two species of a nanocomposite is called compacted type composite, as shown in Fig. 1, where no continuous phase of a single material is formed. Due to the compacted arrangement of interfaces, there is no path that phonons can pass through without being scattered by interfaces. The compacted nanowire periodic two-dimensional (2D) composites may yield even lower thermal conductivity than composites with nanowires embedded in a host material at the same interface density and characteristic size.[17] The further reduction in thermal conductivity can be expected for compacted nanoparticle periodic three-dimensional (3D) composites due to the additional interface scattering in the 3D structures. In this work, we study the thermal conductivity and phonon transport both in compacted 2D nanowire and 3D nanoparticle composites using a deterministic phonon BTE solver. By directly comparing the 2D and 3D compacted nanocomposite structures based on the same parameters, we can assess more precisely the benefit of nanoscale effects on thermoelectric efficiency enhancement.

---

a)Author to whom correspondence should be addressed. Electronic mail: yangjy@spring.iam.ntu.edu.tw.
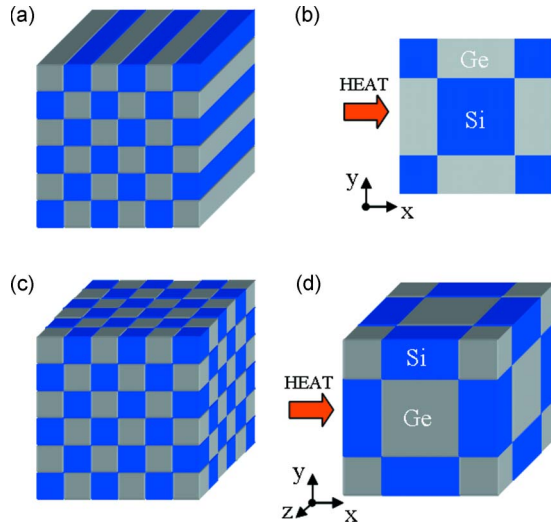
FIG. 1. (Color online) Compacted nanowire and nanoparticle composites. (a) Schematic of a compacted nanowire composite. (b) Unit cell of a compacted nanowire composite for the simulation. (c) Schematic of a compacted nanoparticle composite. (d) Unit cell of a compacted nanoparticle composite for the simulation.

II. THEORETICAL MODEL AND SIMULATION

The heat transport in semiconductors is mainly by phonons and the phonon transport can be well described by the phonon BTE as the length scale is much larger than the phonon coherent length. A phonon gray media approximation is employed in this study where the average phonon properties are used to represent the integral behavior of phonons with different frequency and polarization. The gray medium approximation is found to be a good approximation for the interface-scattering dominant problems[18] and has been applied to a wide range of nanostructures.[6] In this work, the average phonon MFP and the group velocity are used, which are obtained by approximating the dispersion relations of the acoustic phonon branches with simple sine functions and neglecting the heat transfer contribution of the optical phonon branches.[19] We consider the compacted nanowire and nanoparticle composites as shown in Fig. 1. Due to the periodicity of the structure, a unit cell is used to analyze the nanostructure. The characteristic size L_c denotes the width of the square nanowire or the cubic nanoparticle. The width of the unit cell is L. The ratio of L to L_c is 2, which presents for equal atomic composition of the two species composites. To study the phonon heat transfer, a constant temperature difference is applied at the boundaries in the x direction.

The 3D phonon BTE with the Bhatnagar–Gross–Brook (BGK) relaxation time model can be formulated as[20]

$$\frac{\partial I}{\partial t} + \mu \frac{\partial I}{\partial x} + \eta \frac{\partial I}{\partial y} + \zeta \frac{\partial I}{\partial z} = \frac{I_E - I}{\Lambda}, \qquad (1)$$

where (x, y, z) are the Cartesian coordinates, t is time, I is the phonon intensity, I_E is the equilibrium phonon intensity in which phonon distribution function assuming the Bose–Einstein distribution, Λ is the averaged phonon MFP, and μ, η, and ζ are the direction cosines of the phonon direction in the x, y, and z coordinates as shown in Fig. 2. The direction cosines can be expressed as $\mu = \cos\theta$, $\eta = \sin\theta\cos\phi$, and
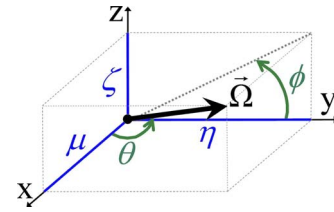

FIG. 2. (Color online) Phonon direction and direction cosines.

$\zeta = \sin\theta\sin\phi$, where θ is the polar angle and ϕ is the azimuthal angle. The phonon intensity is defined by $I = \Sigma_p \int_0^{\omega_p} v_p \hbar\omega f D(\omega) d\omega$, where f is the phonon distribution function, subscript p denotes the phonon polarization, v_p is the phonon group velocity in each polarization, ω is the phonon frequency, ω_p is the maximum frequency in each polarization, $D(\omega)$ is the density of state, and $\hbar$ is the Planck constant divided by 2π.

The phonon intensity is defined as the flux of energy in the direction of phonon propagation per unit area, per unit solid angle. The left-hand side of Eq. (1) represents the free streaming of phonons in space and the right-hand side denotes the collision term. In the BGK approximation, the collision operator involves simple relaxation to a local equilibrium state. The phonon intensity I and the equilibrium phonon intensity I_E satisfy the conservation constraint. The equilibrium phonon intensity can be represented by phonon intensity as

$$I_E = \frac{1}{4\pi} \int_\Omega I d\Omega, \qquad (2)$$

where Ω is the solid angle of the phonon direction.

There are two main mechanisms contributing to thermal resistances in phonon transfer in nanostructures. One is due to intrinsic scattering and the other interface scattering. The intrinsic scatterings including impurity scattering, phonon-phonon scattering, and phonon-electron scattering are lumped through the averaged MFP estimated from the experimental data. When a phonon encounters an interface formed by different materials, the phonon may experience specular[21] or diffuse[22] scattering. The type of interface scattering depends on the surface roughness of the interface and the coefficients for specular reflection are given by Ziman.[23] The diffuse mismatch model[22] assumes that phonons emerging from the interface do not really bear any relationship with their origin. At room temperature, the phonon scattering event at the interface can be regarded as fully diffuse scattering. Most of the experimental results show that diffuse scattering dominates phonon transport in nanostructures. In this work, the interface scattering is assumed to be diffuse. A detailed balance consideration leads to the following definition of energy transmissivity for diffuse interface:[24]

$$T_{12} = \frac{U_2 v_2}{U_1 v_1 + U_2 v_2}, \qquad (3)$$

where T_{12} is the phonon transmissivity across the interface from medium 1 to medium 2, U is the phonon energy density, and v is the average phonon velocity. The subscripts represent different media. Under the diffuse mismatch

model, the relation for transmissivity and reflectivity is $T_{12} = R_{21} = 1 - T_{21}$. With the transmissivity and reflectivity given, the phonon intensity in the outward direction (leaving the interface) at the interface can be calculated by phonon intensity in the inward direction (incoming to the interface). As an example, the phonon intensity at interface ($x = L_c/2$, $0 \leq y \leq L$, $0 \leq z \leq L$) in the unit cell of the compacted nanoparticle composite is used to explain the interface condition. From the energy balance condition and isotropic scattering assumption, the phonon intensity in the outward direction ($\mu > 0$) at right-hand side of the interface can be expressed as

$$I\left(\frac{L_c^+}{2}, y, z, \mu, \phi\right) = \frac{T_{12}}{\pi} \int_0^{2\pi} \int_0^{+1} \mu I\left(\frac{L_c^-}{2}, y, z, \mu, \phi\right) d\mu d\phi$$
$$+ \frac{R_{21}}{\pi} \int_0^{2\pi} \int_{-1}^{0} \mu I\left(\frac{L_c^+}{2}, y, z, \mu, \phi\right) d\mu d\phi, \tag{4}$$

where the superscripts $+$ and $-$ indicate the positions on the right and left sides of the interface, respectively. The phonon intensity at the left-hand side of the interface, in outward direction ($\mu < 0$), can be formulated correspondingly. The phonon intensities at other interfaces can be similarly formulated.

For the boundary conditions of the unit cell, the periodic boundary condition is used due to the periodicity of the structure. In the planes that are parallel to the heat flow x-direction, the implementation of periodic boundary condition is simple. As an example, we consider the boundary ($0 \leq x \leq L$, $y = 0$, $0 \leq z \leq L$) in the unit cell of the compacted nanoparticle composite. The phonon intensity in the outward direction ($\eta > 0$) at each point of the boundary is assigned as

$$I(x, y = 0, z, \mu, \phi) = I(x, y = L, z, \mu, \phi). \tag{5}$$

Similar expressions can be given for the boundary ($0 \leq x \leq L$, $y = L$, $0 \leq z \leq L$) with ($\eta < 0$) and similarly for the $z = 0$ and $z = L$ unit cell planes.

In the planes that are normal to the heat flow x direction, the implementation of periodic boundary condition has to be corrected due to the existence of a fixed temperature difference, which caused a distortion in the phonon intensity.[10] To implement the periodic boundary condition, one requires that the distortion of phonon intensity in each direction at each point of the boundary $x = 0$ is the same as the distortion in the corresponding direction at the corresponding point of the $x = L$ boundary. Thus, for the phonon intensity in the outward direction ($\mu > 0$) at the boundary plane ($x = 0$, $0 \leq y \leq L$, $0 \leq z \leq L$), we set

$$I(x = 0, y, z, \mu, \phi) - I_E(x = 0, y, z) = I(x = L, y, z, \mu, \phi)$$
$$- I_E(x = L, y, z). \tag{6}$$

Similarly, one can specify the condition at $x = L$ unit cell plane.

At the nanoscale, temperature can no longer be defined in a usual manner and one has to use the effective temperature to reflect the local energy density inside the medium. The equivalent temperature can be expressed with phonon intensity as

$$T = \frac{1}{4\pi C v} \int_\Omega I d\Omega = \frac{I_E}{C v}, \tag{7}$$

where T is equivalent temperature, C is the specific heat of the material, and v is the phonon velocity.

The heat flux in the x direction can be presented as

$$q = \int_\Omega \mu I d\Omega. \tag{8}$$

A deterministic numerical method based on finite-difference method in physical coordinates and discrete order method in angle coordinates for solving the phonon Boltzmann equation is employed. The advantage of using the deterministic phonon BTE solver over MC method is that the latter normally costs much more computer time to get a statistically reasonable answer. Here in the present direct phonon BTE solver, the discrete ordinate method and step scheme[20,25] with parallel implementation[15,26] are employed to solve Eq. (1). For angular discretization, the total solid angle Ω is divided into some discrete directions. To achieve high-order integration accuracy, Gauss–Legendre (GL) quadratures are used to discretize $\mu(-1 \sim +1)$ and $\phi(0 \sim 2\pi)$ into certain points decided by the quadrature rule. The integration over the solid angle can be calculated by the summation of function value in each discrete direction $\vec{\Omega}_{m,n} = (\mu_m, \phi_n)$ multiplying its corresponding weights w_m and ϖ_n. The equilibrium phonon intensity can be represented as

$$I_E = \frac{1}{4\pi} \int_\Omega I d\Omega = \frac{1}{4\pi} \sum_{m=1}^{N_\mu} \sum_{n=1}^{N_\phi} w_m \varpi_n I_{m,n}, \tag{9}$$

where the subscripts m and n represent the phonon directions.

With discrete phonon directions specified, the original governing equation can be transferred into a set of differential equations in each phonon direction,

$$\frac{\partial I_{m,n}}{\partial t} + \mu_m \frac{\partial I_{m,n}}{\partial x} + \eta_{m,n} \frac{\partial I_{m,n}}{\partial y} + \zeta_{m,n} \frac{\partial I_{m,n}}{\partial z} = \frac{I_E - I_{m,n}}{\Lambda}. \tag{10}$$

The above set of equations can be numerically integrated using the step scheme in space and backward Euler scheme in time as

$$\frac{I_{i,j,k,m,n}^{s+1} - I_{i,j,k,m,n}^{s}}{\Delta t} \mp \mu_m \frac{I_{i\mp1,j,k,m,n}^{s+1} - I_{i,j,k,m,n}^{s+1}}{\Delta x}$$
$$\mp \eta_{m,n} \frac{I_{i,j\mp1,k,m,n}^{s+1} - I_{i,j,k,m,n}^{s+1}}{\Delta y} \mp \zeta_{m,n} \frac{I_{i,j,k\mp1,m,n}^{s+1} - I_{i,j,k,m,n}^{s+1}}{\Delta z}$$
$$= \frac{I_{Ei,j,k}^{s} - I_{i,j,k,m,n}^{s+1}}{\Lambda}, \tag{11}$$

where the superscript s is the time step index, the subscripts i, j, and k are the indices in x, y, and z coordinates, and m and n are discrete indices of μ and ϕ, respectively. Δt is the time step size and Δx, Δy, and Δz are mesh sizes in x, y, and

z coordinates. The symbols $\mp$ in Eq. (11) are decided by the signs of direction cosines in x, y, and z coordinates, respectively. The phonon direction with $\mu_m > 0$, $\eta_{m,n} < 0$, and $\zeta_{m,n} > 0$ is used as an example. In this case, according to the step scheme, both symbols $\mp$ in the second term of Eq. (11) assume minus sign, the symbols $\mp$ in the third term assume plus sign, while both symbols $\mp$ in the fourth term assume minus sign. The formula for other directions can be similarly defined.

With the phonon intensity $I_{m,n}^s$ in each direction at time step s known, the value of phonon equilibrium intensity I_E^s is calculated from Eq. (9). Then the phonon intensity $I_{m,n}^{s+1}$ in each direction at next time step can be calculated with Eq. (11). At the location of interface and boundary of the unit cell, the phonon intensity in outward direction is calculated by the diffuse interface condition or periodic boundary condition. Special attention should be paid to the arrangement of materials 1 and 2 inside the unit cell of compacted type nanocomposite. Because implicit time discretization is used, the time step size is not limited.[27] This can greatly reduce the total number of time step needed in a steady state problem. The procedure is repeated until the steady state is reached. The steady state solution of phonon intensity $I_{m,n}$ is solved by iteration over the equilibrium phonon intensity I_E. The solution is assumed to be convergent when the maximum relative difference of the equilibrium phonon intensity between two iteration steps is less than 10^{-6}. The steady state temperature and heat flux can be calculated by numerically integrating Eqs. (7) and (8) with GL quadratures. With the similar definition of Fourier law, the effective thermal conductivity can be calculated by $k_e = \bar{q}L/\Delta T$, where ΔT is the temperature difference applied at boundaries in x direction and the average heat flux $\bar{q} = \iint q \, dy \, dz / L^2$. The following dimensionless parameters are used in the numerical simulation:

$$\hat{x} = \frac{x}{L}, \quad \hat{y} = \frac{y}{L}, \quad \hat{z} = \frac{z}{L},$$

$$\hat{T} = \frac{T - T_0}{\Delta T}, \quad \hat{q} = \frac{q}{C_0 v_0 \Delta T}, \quad (12)$$

where C_0 is the specific heat of germanium and v_0 is the sound speed in germanium. The reference temperature T_0 is 300 K and the constant temperature difference ΔT is 1 K.

III. RESULT AND DISCUSSION

The parameters of silicon (Si) and germanium (Ge) at temperature 300 K used in the simulations are directly taken from Yang and Chen.[10] The bulk thermal conductivity of silicon is 150 W/mK and germanium is 60 W/mK. For the 2D compacted nanowire structure, the x directional cosine μ direction is discretized into $N_\mu = 80$ points by GL quadrature from -1 to $+1$ and the ϕ direction is discretized into $N_\phi = 30$ points with GL quadrature from 0 to π (not 0 to 2π due to symmetry). A uniformly spaced Cartesian spatial grid system of size $N_x = 150$ and $N_y = 150$ is used within the square unit cell. To ensure grid convergence of the solution procedure, a finer mesh system is also used. The maximum relative difference of the effective thermal conductivity with

finer mesh $N_x = 200$, $N_y = 200$, $N_\mu = 120$, and $N_\phi = 50$ is found to be less than 0.5%. For the 3D compacted nanoparticle structure, μ is discretized into $N_\mu = 80$ points by GL quadrature from -1 to $+1$ and ϕ is discretized into $N_\phi = 60$ points with GL quadrature from 0 to 2π. A uniformly spaced Cartesian spatial grid system of size $N_x = 150$, $N_y = 150$, and $N_z = 150$ is used in the x, y, and z coordinates within the cubic unit cell. To ensure the grid convergence of the steady state solution, we also simulated the same problem with a finer grid system with $N_x = 200$, $N_y = 200$, $N_z = 200$, $N_\mu = 120$, and $N_\phi = 100$. The maximum relative difference of the effective thermal conductivities between the two grid systems is less than 0.5%.

Figure 3 shows the steady state temperature and heat flux distributions within the square unit cell of Si–Ge compacted nanowire composites with characteristic size (the width of the wire) of 3 nm. Due to the nature of the present deterministic phonon BTE solver, the temperature and heat flux distributions can be clearly obtained. From Figs. 3(a) and 3(b), temperature overshooting at the interfaces and around the nanowire corners in embedded nanowire composites reported by Yang and Chen[10] no longer appears in compacted nanowire composite. Due to the compact interface arrangement (phonons cannot pass through without being scattered) in compacted type nanocomposite, the energy of phonons cannot accumulate to form the local maximum or minimum within the medium and the temperature distribution inside the medium is more uniform. The temperature distribution is symmetric along the $y = L/2$ line. The temperature jump as created by the large thermal resistance across the cross-plane (located at $x = 0.25$ and $x = 0.75$) interface between the silicon and germanium is clearly captured, as shown in Fig. 3(b). The smaller temperature jump in in-plane interfaces (located at $y = 0.25$ and $y = 0.75$) is also obtained. The reason for smaller jump is that the phonon heat transfer is mainly in the x direction (along the applied temperature-difference direction) and the phonon energy loss in the y direction is smaller due to fewer phonons moving in this direction. We can observe that the value of heat flux near the in-plane interface is lower than other regions [shown in Fig. 3(c)]. The in-plane interfaces cause restrictions on the motions of phonons. Also as an example to validate the present method, the thermal conductivities of Si–Ge compacted nanowire composites are compared with those obtained by MC method.[17] The agreement is excellent and the relative percentage deviation is less than 3% [shown in Fig. 4(b)].

Figure 5 shows the steady state temperature and heat flux distribution distributions within the cubic unit cell of Si–Ge compacted nanoparticle composites with characteristic size (the width of the particle) of 3 nm. From Figs. 5(a) and 5(b), it is found that temperature overshooting at the interfaces and around the nanoparticle corners in embedded nanoparticle composites[15,16] no longer appears in compacted nanoparticle composites. The temperature distribution is symmetric with respect to the $y = L/2$ plane. Again, the temperature jump caused by large thermal resistance across the cross-plane interface (located at $x = 0.25$ and $x = 0.75$) is clearly captured as shown in Fig. 5(b). The smaller tempera-
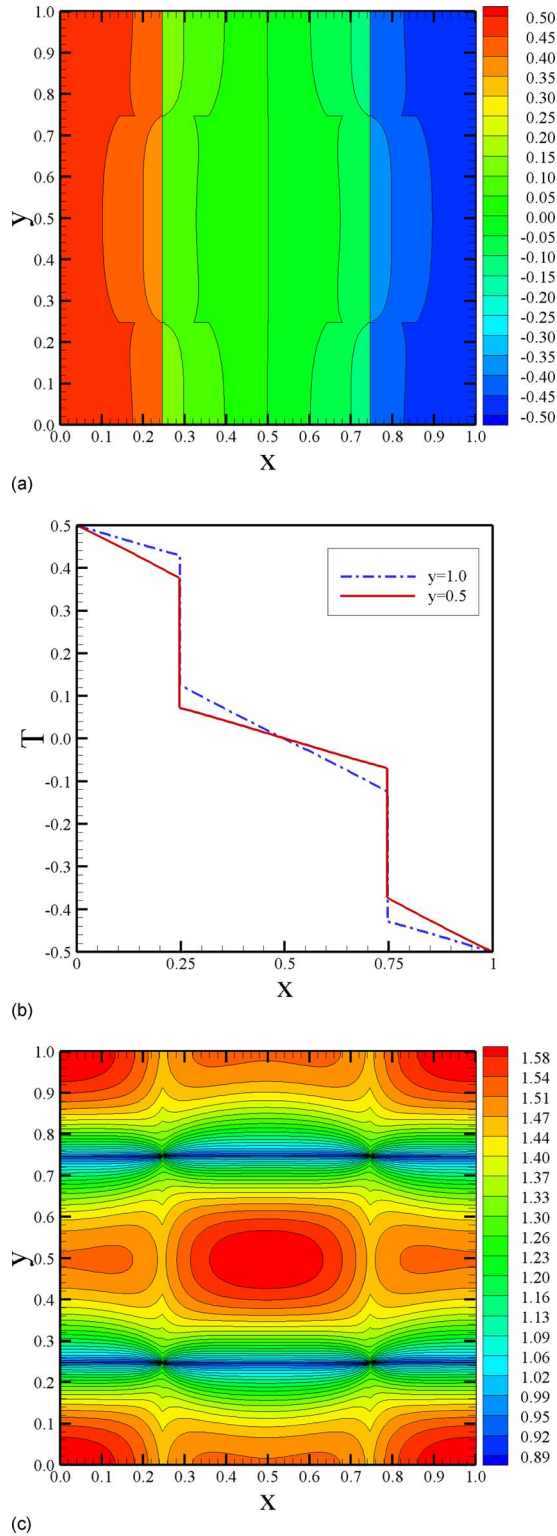
(a)

(b)

(c)

FIG. 3. (Color online) The silicon-germanium compacted nanowire composite. (a) Temperature distribution within the unit cell. (b) Temperature distribution along x at $y=0.5$ and $y=1.0$. (c) Heat flux distribution within the unit cell. The width of the nanowire is 3 nm.
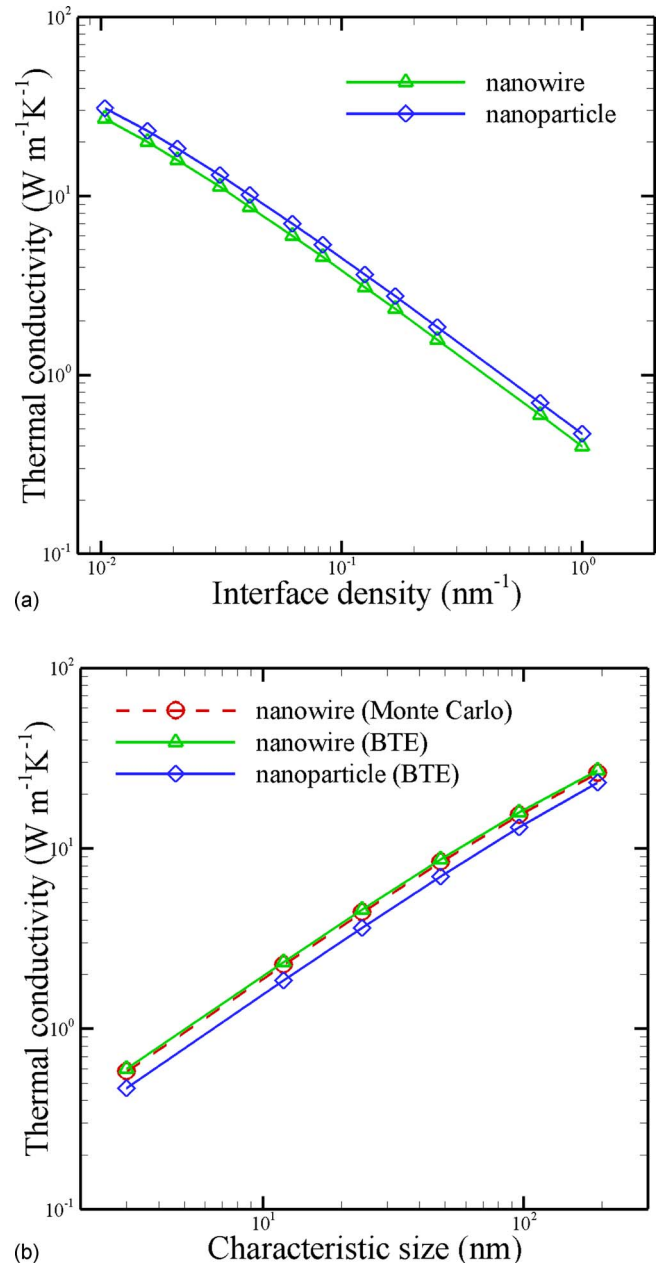

(a)

(b)

FIG. 4. (Color online) Comparison of thermal conductivity of silicon-germanium compacted nanowire and nanoparticle composites. (a) Effects of different interface densities. (b) Effects of different characteristic sizes.

ture jump in in-plane interfaces (located at $y=0.25$, $y=0.75$, $z=0.25$, and $z=0.75$) is also obtained. The lower value of heat flux near the in-plane interfaces is observed [shown in Fig. 5(c)]. In addition, we compare the temperature distributions of compacted nanowire and nanoparticle composites and observe that the temperature gradient is larger in the

nanoparticle structure. The reason is that two more in-plane interfaces (located at $z=0.25$ and $z=0.75$) exist in the nanoparticle composite and the phonon energy is affected by these two additional interfaces. We compare the heat flux distributions in compacted nanowire and nanoparticle composites and observe that the maximum and minimum values are lager in the nanowire composite. These results show that phonons can pass through the nanowire structure with less resistance than passing through the nanoparticle structure.

To analyze the phonon heat transfer in compacted type nanocomposites, the interface density is used to illustrate the effect of interface scattering. The interface density is defined as the area of interfaces divided by the volume of the unit cell. For a characteristic size L_C, the interface densities of compacted nanowire and nanoparticle composites are $2/L_C$
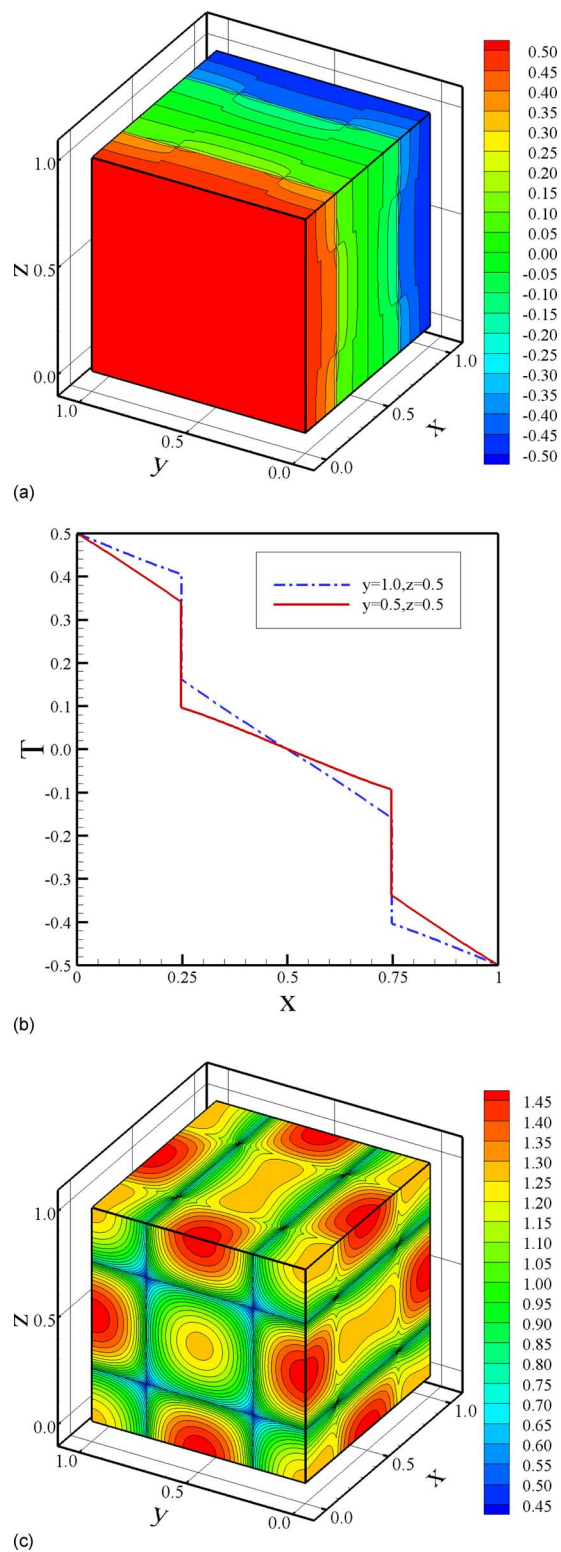
(a)

(b)

(c)

FIG. 5. (Color online) The silicon-germanium compacted nanoparticle composite. (a) Temperature distribution within the unit cell. (b) Temperature distribution along x at $y=0.5$ and $y=1.0$ in the middle plane of the z coordinate ($z=0.5$). (c) Heat flux distribution within the unit cell. The width of the nanoparticle is 3 nm.

and $3/L_C$. A comparison of thermal conductivities of compacted nanowire and nanoparticle composites for various interface densities is shown in Fig. 4(a). The interface density used in the phonon BTE simulations is ranging between 1 and 0.01 nm^{-1}. Apparently, the thermal conductivity of the

nanowire composite is lower than that of the nanoparticle composite for the same interface density. The interface-scattering efficiency of nanoparticle structure is lower. The interface-scattering efficiency is affected by the ratio of cross-plane interface area to that of in-plane interface. The interface area is more efficient for phonon scattering by cross-plane interface.[10] The compacted nanowire composite contains half of its interface area in the cross-plane direction and the other half in the in-plane direction, while the compacted nanoparticle composite contains only one-third of its interface area in the cross-plane direction. Similar observation for embedded type nanocomposites was discussed by Jeng *et al.*[16] The effect of interface scattering becomes more obvious when the percentage of cross-plane interface is higher. The one-dimensional superlattice structure is the limiting case that all interfaces are cross-plane interface. Due to more intrinsic scattering is included when interface density is decreased, the effect of interface scattering becomes less dominant and the relative difference of thermal conductivity between nanowire and nanoparticle composites is reduced. The relative difference in thermal conductivity between nanowire and nanoparticle is 14.8% lower when interface density is 1 nm^{-1} and 12.8% lower when interface density is 0.01 nm^{-1}. Although the interface-scattering efficiency is lower in 3D structure, the characteristic sizes of nanowire and nanoparticle are different for the same interface density. The width of the nanoparticle is one and a half times of that of the nanowire. Apparently, the interface density for compacted nanoparticle composites is 50% more than that of compacted nanowire composites under the same characteristic size. This could be a desirable property of 3D structure. For the length scale limit that the current manufacturing technique can still produce, the nanoparticle structure can have higher interface density than nanowire structure. Under the same characteristic size (width of wire or particle), the thermal conductivities of these two composites are plotted in Fig. 4(b). The characteristic size used in the phonon BTE simulation is ranging between 3 and 192 nm. It is observed that nanoparticle composites can achieve lower value of thermal conductivity than that of nanowire. The higher interface density of compacted nanoparticle composite is a promising feature for thermal conductivity reduction. Due to more intrinsic scattering can be included as the characteristic size is increased and the effect of interface scattering becomes less dominant, consequently the relative difference in thermal conductivity between compacted nanowire and nanoparticle composites is reduced. The relative difference in thermal conductivity is 21.6% lower when the characteristic size is 3 nm and 14.5% lower when characteristic size is 192 nm.

IV. CONCLUSION

We investigated the phonon heat transport and the thermal conductivity in compacted nanowire and nanoparticle composites for various characteristic sizes and interface densities using a deterministic phonon Boltzmann equation solver. With carefully tracing the phonon motion, energy transport in nanostructures with interfaces can be adequately simulated by the phonon BTE solver. The advantage of com-

pacted type nanocomposites is clearly delineated due to its uniform interface arrangement. The thermal conductivity of the Si–Ge compacted nanoparticle composites can be further substantially reduced than that of the Si–Ge compacted nanowire composites at the same characteristic size. Specifically, when the characteristic size is 3 nm, the thermal conductivity of the Si–Ge compacted nanoparticle composites is found to be 21.6% lower than that of the nanowire type. The 3D nanocomposites have the advantage for scaling up larger interface density that can be very beneficial for enhancing the thermoelectric figure of merit *ZT* of thermoelectric devices.

ACKNOWLEDGMENTS

[1]K. E. Goodson and Y. S. Yu, Annu. Rev. Mater. Sci. **29**, 261 (1999).
[2]G. Chen, Semicond. Semimetals **71**, 203 (2001).
[3]D. G. Cahill, W. K. Ford, K. E. Goodson, G. D. Mahan, A. Majumdar, H. J. Maris, R. Merlin, and S. R. Phillpot, J. Appl. Phys. **93**, 793 (2003).
[4]A. Majumdar, Science **303**, 777 (2004).
[5]C. Kittel, *Introduction to Solid State Physics* (Wiley, New York, 1996).
[6]G. Chen, *Nanosclae Energy Transport and Conversion* (Oxford University Press, Oxford, 2005).
[7]R. Venkatasubramanian, E. Siivola, T. Colpitts, and B. O'Quinn, Nature (London) **413**, 597 (2001).
[8]T. C. Harman, P. J. Taylor, M. P. Walsh, and B. E. LaForge, Science **297**, 2229 (2002).
[9]M. S. Dresselhaus, G. Chen, M. Y. Tang, R. G. Yang, H. Lee, D. Wang, Z. Ren, J. P. Fleurial, and P. Gogna, Adv. Mater. (Weinheim, Ger.) **19**, 1043 (2007).
[10]R. Yang and G. Chen, Phys. Rev. B **69**, 195316 (2004).
[11]R. G. Yang, G. Chen, and M. S. Dresselhaus, Phys. Rev. B **72**, 125418 (2005).
[12]R. Prasher, J. Appl. Phys. **100**, 064302 (2006).
[13]R. Prasher, J. Appl. Phys. **100**, 034307 (2006).
[14]W. X. Tian and R. G. Yang, Appl. Phys. Lett. **90**, 263105 (2007).
[15]T.-Y. Hsieh, Ph.D. thesis, National Taiwan University, 2007.
[16]M. S. Jeng, R. G. Yang, D. Song, and G. Chen, ASME Trans. J. Heat Transfer **130**, 042410 (2008).
[17]W. X. Tian and R. G. Yang, J. Appl. Phys. **101**, 054320 (2007).
[18]G. Chen, Phys. Rev. B **57**, 14958 (1998).
[19]G. Chen, ASME Trans. J. Heat Transfer **119**, 220 (1997).
[20]A. Majumdar, ASME Trans. J. Heat Transfer **115**, 7 (1993).
[21]W. A. Little, Can. J. Phys. **37**, 334 (1959).
[22]E. T. Swartz and R. O. Pohl, Rev. Mod. Phys. **61**, 605 (1989).
[23]J. M. Ziman, *Electrons and Phonons* (Oxford University Press, Oxford, 1985).
[24]C. Dames and G. Chen, J. Appl. Phys. **95**, 682 (2004).
[25]R. G. Yang, G. Chen, M. Laroche, and Y. Taur, ASME Trans. J. Heat Transfer **127**, 298 (2005).
[26]S. Srinivasan, R. S. Miller, and E. Marotta, Numer. Heat Transfer, Part B **46**, 31 (2004).
[27]C. Hirsch, *Numerical Computation of Internal and External Flows* (Wiley, New York, 1988).